atmosphere

MDPI

Article

Transition from a Subaerial to a Subnival Permafrost Temperature Regime Following Increased Snow Cover (Livingston Island, Maritime Antarctic)

Miguel Ramos [1,2,*], Gonçalo Vieira [2], Miguel Angel de Pablo [3], Antonio Molina [4] and Juan Javier Jimenez [1,2]

1 Department of Physics and Mathematics, University of Alcalá, 28805 Alcalá de Henares, Spain; JJAVIERJIMENEZ@telefonica.net
2 Centre of Geographical Studies, IGOT, University of Lisbon, 1600-276 Lisboa, Portugal; vieira@edu.ulisboa.pt
3 Department of Geology, Geography and the Environment, University of Alcalá, 28805 Alcalá de Henares, Spain; miguelangel.depablo@uah.es
4 Centro de Astrobiología (CAB), National Institute of Aerospace Technology, 28850 Torrejón de Ardoz, Spain; amolina@cab.inta-csic.es
* Correspondence: miguel.ramos@uah.es; Tel.: +34-918854917

Received: 6 November 2020; Accepted: 4 December 2020; Published: 8 December 2020

Abstract: The Antarctic Peninsula (AP) region has been one of the regions on Earth with strongest warming since 1950. However, the northwest of the AP showed a cooling from 2000 to 2015, which had local consequences with an increase in snow accumulation and a deceleration in the loss of mass from glaciers. In this paper, we studied the effects of increased snow accumulation in the permafrost thermal regime in two boreholes (PG1 and PG2) in Livingston Island, South Shetlands Archipelago, from 2009 to 2015. The two boreholes located c. 300 m apart but at similar elevation showed different snow accumulation, with PG2 becoming completely covered with snow all year long, while the other remained mostly snow free during the summer. The analysis of the thermal regimes and of the estimated soil surface energy exchange during the study period showed the effects of snow insulation in reducing the active layer thickness. These effects were especially relevant in PG2, which transitioned from a subaerial to a subnival regime. There, permafrost aggraded from below, with the active layer completely disappearing and the efficiency of thermal insulation by the snowpack prevailing in the thermal regime. This situation may be used as an analogue for the transition from a periglacial to a subglacial environment in longer periods of cooling in the paleoenvironmental record.

Keywords: permafrost; active layer; snow thickness; enthalpy

1. Introduction

The analysis of multi-annual permafrost thermal regimes allows determining the energy balance between the soil and the atmospheric boundary layer, which depends on climatic variability, the buffer interfacing between the soil and atmosphere, soil thermophysical properties, and the geothermal gradient [1]. In polar regions, where vegetation cover is scarce or absent, seasonal snow is the main factor generating ground thermal insulation, a key factor for the thermal regime of permafrost [2].

The thermal regime of permafrost in Maritime Antarctica has received increasing research attention since the Fourth International Polar Year (2007–2008), following the installation of several boreholes in the Antarctic Peninsula and nearby islands [3,4]. Those actions are based in the protocol of the programs Circumpolar Active Layer Monitoring (CALM) and Thermal State of Permafrost (TSP) of the International Permafrost Association (IPA), which were initially launched in the boreal regions but were subsequently extended to the Southern Hemisphere [5,6]. The goal of these programs was to install a

network of boreholes with adequate depths to perform direct measurements of ground temperature and thus determine inter annual changes in the permafrost thermal regime, reaching in many cases the depth of zero annual temperature amplitude (ZAA). The measurements of the temperature gradients from these boreholes feed into a global dataset of permafrost temperature time series—the Global Terrestrial Network for Permafrost (GTN-P) to evaluate temperature variability across permafrost regions [4] and to analyse the behaviour of the active layer thickness (ALT). Records of the ground temperature gradient at near-surface and deep levels of a borehole can be used to extract information about the ALT and ZAA, respectively [7]. By assuming that conductive energy fluxes dominate the ground energy balance and that advection is negligible, the profiles of annual maximum and minimum temperatures above the ZAA depth, allow estimating the annual heat exchange between the ground and the lower limit of the atmospheric boundary layer [8].

Our study area is in Livingston Island (South Shetland Islands, Antarctic), in the vicinity of Juan Carlos I Spanish Antarctic Station (BAE JCI). This region has witnessed a marked rise in mean annual air temperature (MAAT) over the past 70 years and is one of the global hot spots of climate warming. MAAT increased by ~+0.56 °C/decade from 1951 to 2000, followed by a statistically significant cooling in the first decade of the 21st century [9,10], with the series showing a new warming trend after 2015 (Figure 1). With MAAT in the South Shetlands at around −2 °C (Bellingshausen station = −2.1 °C for 1981–2010, [10], the region is close to the freezing point of water, and climate change may have a profound effect on the permafrost thermal regime [11].

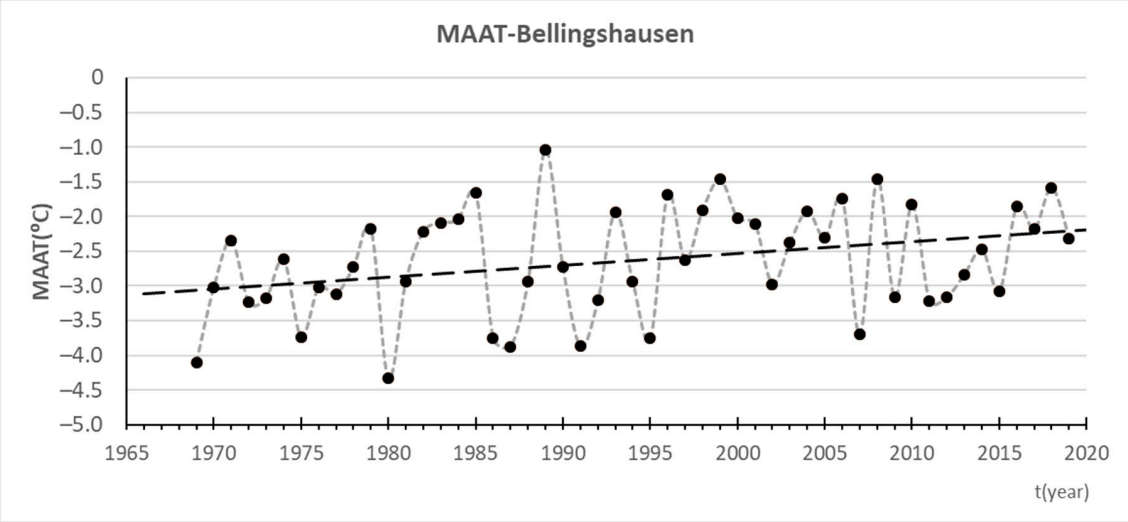

Figure 1. Mean annual air temperature in Bellingshausen station (King George Island) from 1968 to 2020. Data from SCAR Reference Antarctic Data for Environmental Research [12].

From 2009 to 2015, Livingston Island experienced an increase in the duration and thickness of snow cover [13,14], with also a deceleration in the surface mass balance (SMB) losses of Johnsons and Hurd glaciers, noticed when comparing 1957–2000 and 2002–2011. Navarro et al. attribute this decrease to a combination of increased winter snow accumulation and decreased summer melt [15,16]. These changes have also affected lichen communities, which have suffered decreases in cover density and even retreat due to the increased duration of snow cover [17].

We analyse the temperature gradient in two permafrost boreholes (Permamodel-Gulbenkian 1 and 2—PG1 and PG2) drilled in massive quartzite bedrock. The two boreholes are at high-elevation and wind-exposed localities, some 300 m apart and were selected due to the snow-free conditions of the ground during the summer. However, PG2, located close to Hurd Glacier, has become fully snow covered since 2009, with a dense snowpack with multiple ice layers, surpassing 3.5 m in 2015.

The main objectives of this paper are: (i) presenting a comparative study of the inter-annual thermal regime of both boreholes aimed at assessing the thermal effect of the insulating snow pack by analysing the energy exchange using the enthalpy method [8], (ii) expand the understanding on the ground thermal behaviour in the transition stage from a periglacial to a glacial regime in a Maritime Antarctic environment.

2. Study Area

The study area is on Mount Reina Sofia in Hurd Peninsula (Livingston Island, South Shetland Islands) (Figure 2). As part of the Thermal State of Permafrost (TSP) program, launched in the IPY [3], two neighbouring locations have been selected to drill the permafrost boreholes PG1 and PG2, which were equipped with sensors for continuous measurement of the ground temperature gradient. The area was selected, following a detailed assessment of shallow permafrost and active layer temperature [18], as well as geophysical surveys (electrical resistivity tomography and refraction seismics) to characterise permafrost distribution [19].

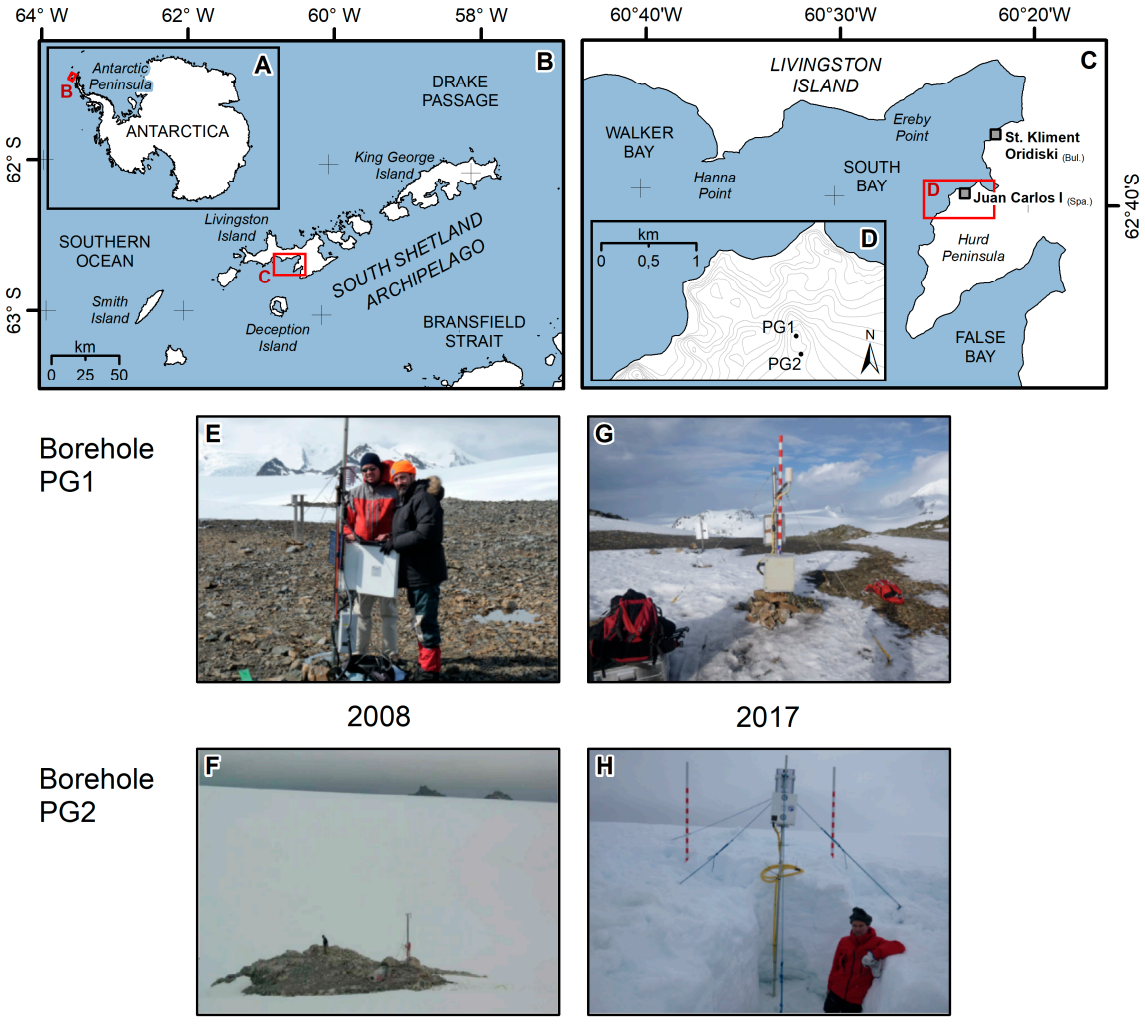

Figure 2. General setup of the permafrost boreholes. (**A**–**D**) Geographical setting of the boreholes in Antarctica, the South Shetlands and in Hurd Peninsula. (**E**) Borehole PG1 in the summer of 2008, (**F**) Borehole PG2 in the summer of 2008, (**G**) Borehole PG1 in the summer of 2017, (**H**) Borehole PG2 in the summer of 2017.

Livingston Island shows a polar maritime climate with frequent precipitation that frequently falls as rain in the summer (annual precipitation = 414 mm), the relative humidity throughout the year is close to saturation especially in the summer (mean annual = 83%), with a MAAT of −1.2 °C at sea-level [20,21]. From November to March, the daily temperature can rise above 0 °C with a mean summer air temperature close to 1.9 °C. The annual maximum temperature recorded at the Spanish Station Juan Carlos I (BAE JCI, 62°39′48″ S, 60°23′19″ W; 13 m a.s.l.) from 1988 to 2014 was 15.5 °C, while the annual minimum temperature was −22.6 °C [20,21].

Mount Reina Sofia is a rocky peak carved in the Myers Bluff Formation, dominated by quartzite and shales, with a surficial frost shattered diamicton showing the development of stone circles [22]. This is the setting of borehole PG1, drilled in the flat summit area, which is mostly snow free in the summer and has only a limited accumulation in winter due to the strong winds [23]. PG2 is located close in a convex rock outcrop in the vicinity to Hurd Glacier, initially snow free, but it has become snow covered all year long since 2009.

The fundamental difference between the boreholes PG1 and PG2 is their exposure to winds from the south that blow the snow from at the summit where PG1 is located, and the susceptibility to the accumulation of snow at PG2 that accumulates snow drift, close to the glacier. Figure 2 illustrates these differences and the snow accumulation from 2008 to 2015. The summit area (PG1) remained virtually snow-free in the summer, with no significant variation during the study period; whereas, PG2 witnessed the formation of an accumulation of ice and snow, which was over 3.5 m thick in 2015 (Figure 2F,H).

3. Methods

3.1. Ground Temperature, Air Temperature, and Snow Thickness

The two boreholes used for the analysis were drilled in February 2008. PG1 is at the top of Reina Sofía Mount (271 m a.s.l.) and is 25 m deep (Figure 2E,G), and PG2, which is 15 m deep, is located in a rock knob close to Hurd Glacier at 255 m a.s.l., about 300 m SSW of PG1 [24] (Figure 2F,H). PG1 has been subject previously to electrical resistivity tomography indicating an ALT of 0.5 to 1.1 m with low electrical resistivity. Down to about 16 m depth, resistivity indicated a rocky zone with low ice content [19]. Both boreholes were drilled in similar quartzite bedrock with thermal conductivity in the range of 2.6 to 3.3 W/m K and thermal diffusivity from 1.1×10^{-6} to 1.6×10^{-6} m^2/s [25]. The boreholes are equipped with long thermometric chains and dataloggers and a similar sensor distance following the TSP protocol [24,26]. In the case of PG1, we used a thermometric chain with 20 measurement levels consisting of YSI 44031 thermistors with an accuracy of ± 0.1 °C (Table 1). This chain was supplemented with an air temperature sensor Vaisala HMP45D (Vaisala Company. Vantaa, Finland) with Pt100 platinum resistance with an accuracy better than ± 0.1 °C, protected with a solar radiation shield, mounted on a mast at a 1.5 m. All the sensors were connected to a CR1000 Data Acquisition System (DAS) via an AM 16/32 multiplexer (Campbell Scientific Ltd. Barcelona, España). Measurements were recorded every 5 min, and mean hourly values were stored. A failure of the PG1 DAS in April 2012 resulted in a loss ground temperature data until the end of 2013, resulting in an incomplete data series during that period.

Table 1. Characteristics of the boreholes PG1 and PG2 and its thermometric chains.

Borehole Name	Coordinates	Altitude (m a.s.l.)	Diameter (mm) (±1 mm)	Depth (m) (±0.02 m)	Sensor Position (m) (±0.005 m)	Sensors Description
PERMAMODEL-GULBENKIAN-1 (PG1)	62.8390° S, 60.8210° W	271	40	25.0	0.2; 0.4; 0.8; 1.2; 1.6; 2.0; 2.5; 3.0; 3.5; 4.0; 5.0; 6.0; 8.0; 10.0; 12.5; 15.0; 17.5; 20.0; 22.5 and 25.0	Thermistors type YSI 44031 (accuracy 0.1 °C) Air temperature Pt100 (accuracy 0.1 °C) Hourly recording
PERMAMODEL-GULBENKIAN-2 (PG2)	62.8390° S, 60.8210° W	255	40	15.0	0.2; 0.4; 0.8; 1.2; 1.6; 2.0; 2.5; 3.0; 3.5; 4.0; 5.0; 6.0; 8.0; 10.0; 12.5 and 15.0	i-button DS1922L (accuracy 0.25 °C) 3 h recording

PG2 is equipped with individual iButton DS1922L (Maxim Integrated. San Jose, CA, USA) miniloggers for each of the 16 measured depths, with an accuracy of ±0.125 °C [27], which recorded simultaneous measurements every 3 h (Table 1).

Snow thickness was measured using two procedures. In PG1, we used thermo-snow-meters [13], allowing us to estimate the snow thickness by analysing the daily variability of air temperature using sensors at different heights in a mast [28]. The resolution of this method depends on the vertical separation between sensors, which in this case were iButton DS1922L miniloggers at 2, 5, 10, 20 40, 80, and 160 cm heights. Despite the low precision of the snow cover heights derived from this method, the results allow for a general overview of the annual snow cover evolution. These data allowed us to estimate the number of days with snow cover and the snow index representing the accumulated daily snow depth in meters, from the day of snow inception to snow melt [28,29]. Snow thickness in PG2 was measured at the time of the summer data collection, in January or February each year, by digging a pit and using a measuring tape with an accuracy of ±2.0 cm.

3.2. Determination of the Active Layer Thickness

The ALT was calculated from the best-fit of the annual maximum temperature profile in the ground (T_M) to a logarithmic equation, allowing us to identify the depth at which the function equals 0 °C. By accounting that maximum (T_M) and minimum annual temperature (T_m) distributions fit logarithmic functions, respectively:

$$T_M(x) = A_M \mathrm{Ln}\, x + B_M \quad (1)$$

$$T_m(x) = A_m \mathrm{Ln}\, x + B_m \quad (2)$$

Table 2a,b shows the fit parameters of the functions that represent the maximum (T_M, 1) and minimum (T_m, 2) annual soil temperature. Applying the condition that shows the interception between the annual maximum temperature and the 0 °C isotherm, we can write:

$$(T_M(x) = A_M \mathrm{Ln}\, X_{ATL} + B_M = 0\ ^\circ\mathrm{C}) \rightarrow X_{ALT} = e^{-\left(\frac{B_M}{A_M}\right)} \quad (3)$$

Table 2. Logarithmic fit parameters for the annual extreme (maximum and minimum) ground temperature profiles for the borehole PG1 (a) and PG2 (b).

(a) PG1 borehole. Sofia peak.						
Year	**A_M (°C)**	**B_M (°C)**	**r^2**	**A_m (°C)**	**B_m (°C)**	**r^2**
2009	−0.80	0.26	0.84	1.63	−6.12	0.91
2010	−0.81	0.20	0.81	1.23	−5.04	0.88
2011	−0.84	0.31	0.78	1.75	−6.62	0.95
2012	No data	No data	No data	No data	No data	No data
2013	No data	No data	No data	No data	No data	No data
2014	−0.44	−0.42	0.94	0.66	−3.61	0.97
2015	−0.43	−0.28	0.72	1.67	−6.55	0.92
(b) PG2 borehole. Glacier margin.						
Year	**A_M (°C)**	**B_M (°C)**	**r^2**	**A_m (°C)**	**B_m (°C)**	**r^2**
2009	−1.92	2.74	0.92	1.78	−6.54	0.95
2010	−1.86	1.97	0.86	1.03	−4.15	0.86
2011	−0.42	−0.26	0.92	1.08	−4.69	0.99
2012	−0.47	−0.31	0.73	0.60	−3.41	0.98
2013	−0.38	−0.49	0.93	0.36	−2.82	0.95
2014	−0.31	−0.60	0.86	0.21	−2.23	0.91
2015	−0.29	−0.52	0.86	0.36	−2.63	0.75

And finally, we obtain the ALT value X_{ALT}.

3.3. Determination of the Zero Annual Amplitude Depth

The maximum and minimum annual temperature at each depth provide information on the annual thermal amplitude. The ZAA was considered to be the depth at which the difference between the maximum and minimum annual temperature is smaller than the accuracy interval of the temperature measurement:

$$T_M - T_m \leq \Delta \text{ (sensor interval accuracy)}$$

where:

$$T_M - T_m = (A_M - A_m)\mathrm{Ln}(x) + (B_M - B_m) = A' \mathrm{Ln}(x) + B' \quad (4)$$

Then:

$$X_{ZAA} = e^{\left(\frac{\Delta - B'}{A'}\right)} \quad (5)$$

3.4. Calculation of the Net Energy Exchange (H)

The annual net energy exchange (H) in the permafrost system was calculated as a function of the area between the logarithmic fit representing the maximum and minimum ground temperature profiles each year as shown in equation (6). The limits of integration are the soil surface of the system (x = 0 m) and the depth of zero annual amplitude (x = X_{ZAA}).

The area between the maximum ($T_M(x)$) and minimum ($T_m(x)$) annual temperature depth functions that have the value of the definite integral of (3) between the limits x = 0 m (soil surface) and x = X_{ZAA}

(position of the zero annual thermal amplitude) determines the integrated annual value of the energy exchange for the soil system across the soil surface, by applying the enthalpic method [8].

$$H(\frac{J}{m^2}) = \frac{K}{\alpha} \int_0^{X_{ZAA}} (T_M(x) - T_m(x))dx \quad (6)$$

Finally:

$$H(\frac{J}{m^2}) = \frac{K}{\alpha}[A' \text{Ln } X_{ZAA} + B' - A']X_{ZAA} \quad (7)$$

where k (W/mK) is the thermal conductivity, and α (m^2/s) is the thermal diffusivity. This procedure allowed us to calculate the energy exchange in both boreholes (H). The analysis of H, ALT, and ZAA allows to estimate the effect of snow insulation by comparing the PG1 and PG2.

4. Results

4.1. Evolution of Air Temperature and Snow Thickness

Mean annual air temperature at Mount Reina Sofia for 2003 to 2015 are shown in Figure 3, with a mean for the period of −4.5 °C, and with −4.2 °C for 2008 to 2015. From 2005 to 2011, MAAT were lower than or close to the mean, while after 2012, MAAT were close to those recorded prior to 2005. The lowest MAAT in the series was in 2007 (−6.5 °C) and the maximum in 2014 (−2.9 °C).

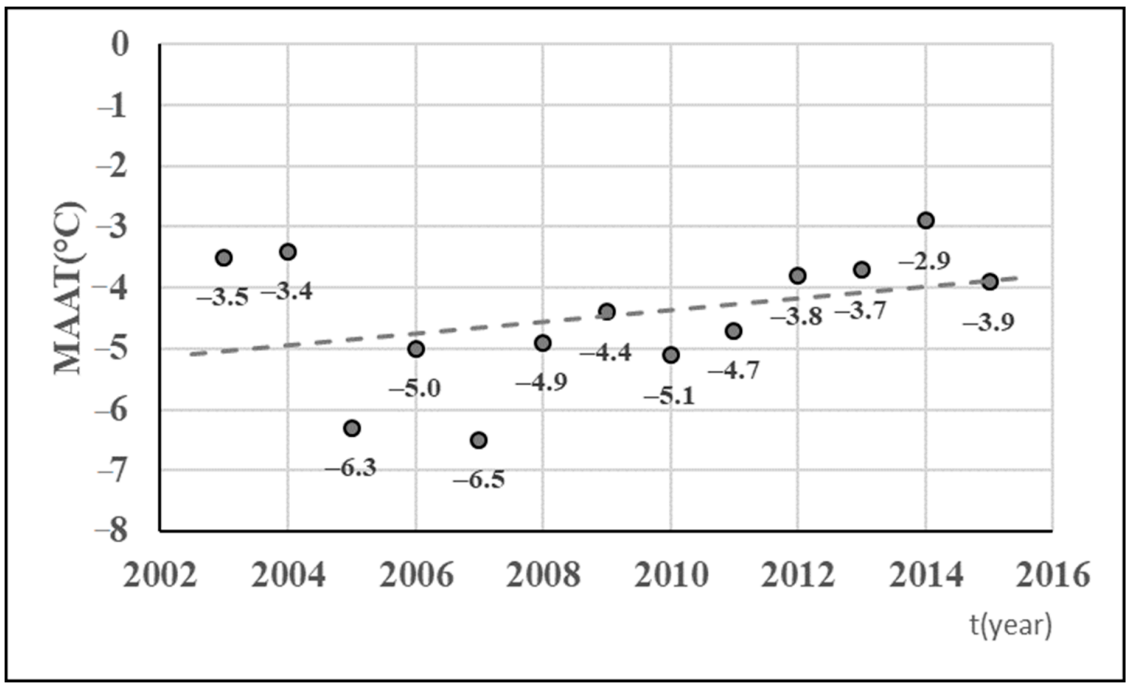

Figure 3. Mean annual air temperature at Reina Sofia Mount (PG1) from 2003 to 2015.

Snow cover at PG1 was characterized by an increment of duration along the period, with an increase in the daily snow depth that reached 40 cm in winter 2013 and spring 2014 to 2016 (Figure 4) and an important increase in the snow index (Table 3), from the autumn of 2012 to 2015, coinciding with the increase in MAAT (Figure 3). On the other hand, PG2 showed a steady annual increase in snow thickness (Table 3), from a snow-free surface in the summer of 2008 when the borehole was drilled to a 3.5 m thick pack of permanent snow early in 2016. This increase in snow accumulation has also been recorded over the neighbour Hurd Glacier [15,30].

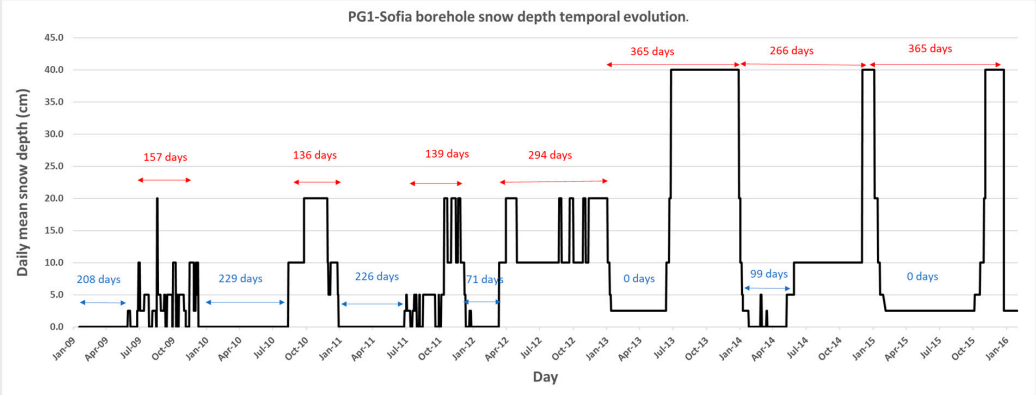

Figure 4. Snow thickness in PG1 from 2009 to 2015.

Table 3. Characteristics of the snow cover thickness at the two borehole sites (m·day).

PG1				PG2	
Year	**Days with Snow Cover**	**Snow Index (m. day)**	**Snow Thickness (Annual Mean) (m)**	**Measuring Date**	**Snow Thickness (Annual Maximum) (±0.02 m)**
2008	No data	No data	No data	15/01/2009	0.00
2009	157	33.8	0.02	09/01/2010	0.40
2010	136	32.9	0.04	10/01/2011	1.40
2011	139	32.4	0.02	08/01/2012	1.84
2012	294	71.0	0.16	15/01/2013	No data
2013	365	87.4	0.10	29/01/2014	2.10
2014	266	63.9	0.09	29/01/2015	2.98
2015	365	93.8	0.08	13/02/2016	3.54

4.2. Active Layer Thickness

Table 4 shows the estimated active layer depth from 2009 to 2015 in both boreholes. In the beginning of the period, PG1 showed an active layer of 1.4 m, while PG2 showed 4.2 m. In the following years, the active layer thickness decreased continuously in PG2, while in PG1, it was stable until 2012, then decreasing in 2014 and 2015. The active layer thickness in 2015 was 0.5 m in PG1 and 0.2 m in PG2. Figure 5 shows the ALT in both boreholes in 2009, 2011, and 2014 and evidences the lack of active layer in PG2 in 2014, as a result of the increased thermal insulation induced by the accumulated snowpack.

Table 4. Active layer thickness for boreholes PG1 and PG2 from 2009 to 2015.

Year	**Active Layer Depth (m)**	
	PG1	**PG2**
2009	1.4 ± 0.4	4.2 ± 0.8
2010	1.3 ± 0.4	2.9 ± 0.4
2011	1.4 ± 0.4	0.5 ± 0.2
2012	1.4 ± 0.4	0.5 ± 0.2
2013	No data	0.3 ± 0.2
2014	0.4 ± 0.2	0.1 ± 0.2
2015	0.5 ± 0.3	0.2 ± 0.3

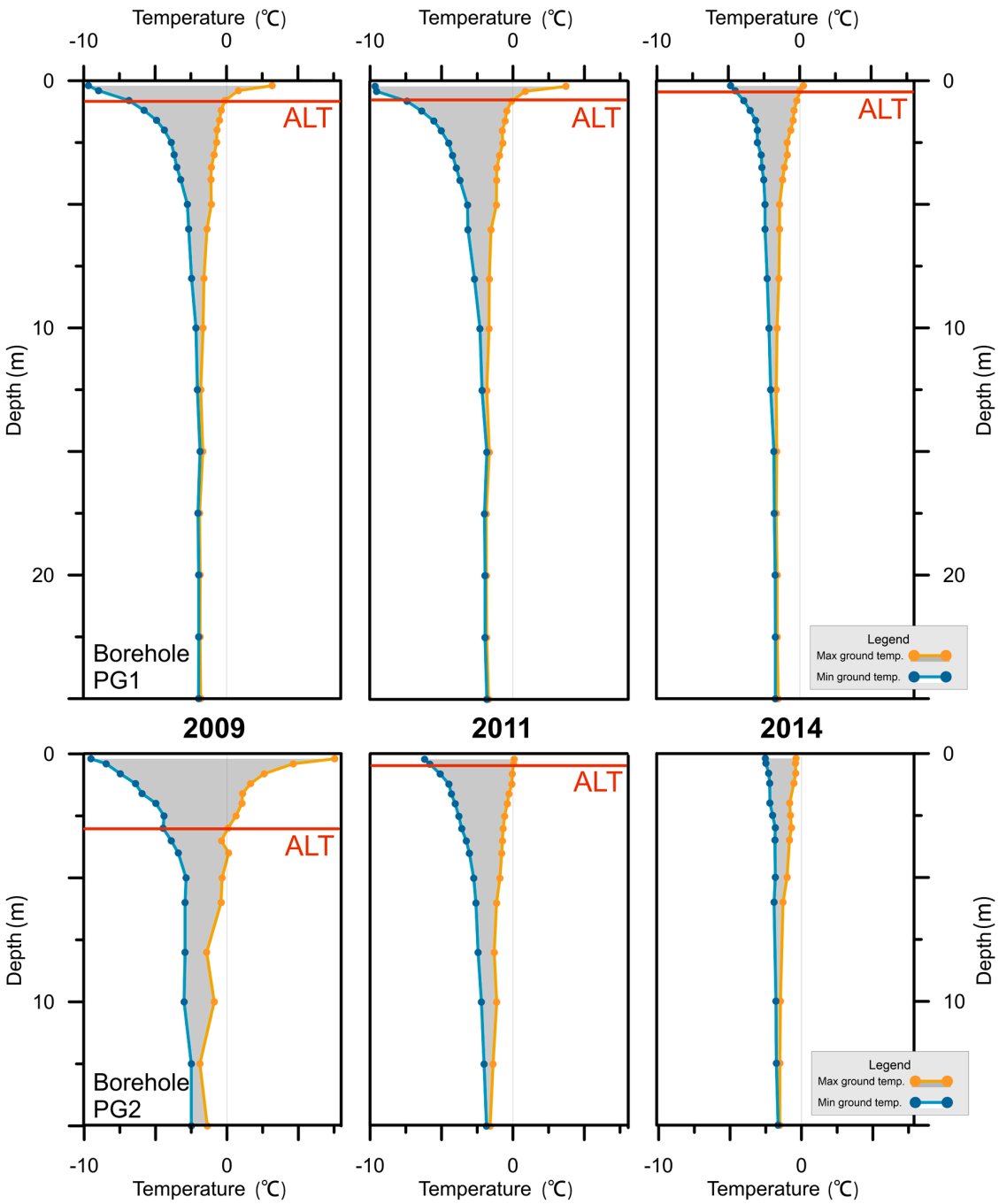

Figure 5. Maximum and minimum ground temperature and active layer thickness in PG1 and PG2 in three selected years (2009, 2011, and 2014).

4.3. Zero Annual Ground Thermal Amplitude (ZAA)

Table 5 shows the estimated ZAA following Equation (5). The ZAA calculated for PG1 varied between 8.5 and 16.4 m with most years showing values close to 12 m, which resulted in a mean value of X_{ZAA}=12 m. On the other hand, the ZAA for PG2 showed a variability conditioned by the insulating snow layer, with a decreasing trend reaching a depth close to the soil surface with a minimum value of 3.3 m (Table 5). The large error is associated to the proximity to the surface and accuracy of the sensors (i-button DS1922L with accuracy of ± 0.25 °C), but the trend towards a shallowing ZAA is clear, as also shown by the temperature data.

Table 5. Zero thermal annual amplitude depth (ZAA) at boreholes PG1 and PG2.

Year	ZAA (PG1)	ZAA (PG2)
	X_{ZAA}(m)	X_{ZAA}(m)
2009	11.8 ± 2.5	9.4 ± 0.7
2010	10.8 ± 2.8	5.9 ± 0.5
2011	12.5 ± 2.5	9.8 ± 1.8
2012	8.5 ± 2.5	7.0 ± 1.8
2013	No Data	6.1 ± 2.2
2014	12.8 ± 6.1	3.3 ± 1.7
2015	16.4 ± 4.1	5.5 ± 2.3

4.4. Soil Surface Energy Exchange

Table 6 shows the results of the application of Equation (7) for PG1 and PG2, expressed in total energy exchange (H) (MJ/m^2) in the annual periods. The soil surface energy exchange shows no trend from 2009 to 2015 in PG1 with values varying from 35 to 78 MJ/m^2. On the other hand, PG2 shows a continuous decreasing of H, with a trend of approximately −10 MJ/m^2 per year, with values varying from 75 to 6 MJ/m^2 from 2009 to 2015 (Figure 6).

Table 6. Annual integration of soil surface energy exchange (H) for PG1 and PG2 boreholes.

Year	H (MJ/m^2) PG1	H (MJ/m^2) PG2
2009	64 ± 7	75 ± 6
2010	50 ± 7	38 ± 4
2011	71 ± 7	38 ± 9
2012	35 ± 5	21 ± 7
2013	No data	14 ± 7
2014	37 ± 10	6 ± 5
2015	78 ± 10	12 ± 7

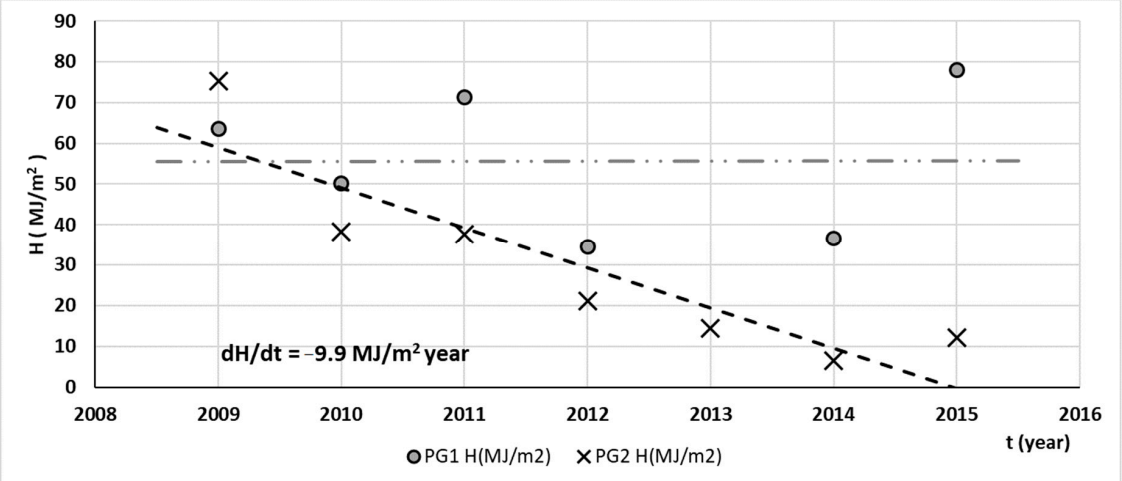

Figure 6. Soil surface energy exchange in PG1 and PG2 from 2009 to 2015 (note that there are no data in PG1 for 2013).

5. Discussion

In Antarctica, the insulating effect of snow cover is the key buffer factor between the soil and the atmosphere, which is emphasized by the limited vegetation cover. This has led to the development of studies on the effects of snow cover on permafrost [31] and on the active layer [32,33], showing a decreasing active layer thickness with increasing duration of snow cover. Other studies have focused on the effect of snow cover on the shallow soil temperatures by comparing freezing and thawing indexes, also revealing the buffering effect of snow and its effect in reducing both indexes [13,34]. The present case study deals with the analysis of how two sites with permafrost and similar initial snow conditions developed very different thermal regimes following a series of years with extreme snow cover. We further contribute to the body of research by introducing a quantitative analysis of the total energy exchanged across the soil surface under different snow covers.

The complete disappearance of the active layer at PG2 was produced by the thermal insulation above the ground generated by an accumulation of snow, which was thick enough to reduce the thermal flux between the soil surface and the atmospheric boundary layer. At this site, the ground thermal regime moved from conditions in which the energy exchange with the atmosphere prevailed, to another in which the thermal regime depends almost exclusively on the geothermal heat flux (influence of the cooler permafrost at depth). Here, we should note that method used to determine H is based on the measurement of the difference in soil temperature between the annual maxima and minima. When the differences between the maxima and minima are small, the measurement errors increase, especially when H tends to zero due to snow accumulation (Table 6).

In the case of PG1, an increase in snow accumulation is observed starting in the winter of 2012, leading to a persisting snowpack from 2013 to 2015. This increasingly thick snowpack generated a thermal insulation effect that resulted in a thinning of the active layer and in a decrease in the energy exchange (H, Tables 4 and 6), which was more pronounced in 2012 and 2014.

PG2 presented a completely different evolution than PG1. The total annual energy exchange (H) has shown a steady reduction over time, indicating a decrease in energy exchange with the atmosphere due to the thermal insulation provided by the permanent layer of snow that accumulated on the soil surface (Figure 6). This perennial snow began to develop in 2009 and grew steadily thicker until reaching its maximum value of 3.54 m in early 2016 (Table 3). In this case, H steadily dropped from 2009 to 2014, following the reduction in soil annual temperature amplitude. Values in 2014 and 2015 were similar, reflecting the thermal isolation of the permafrost system from the atmospheric boundary layer and considering the accuracy of the method (Figure 6). This resulted in the disappearance of the active layer and on progressive permafrost aggradation towards the surface, with cooling from below. The maximum temperature of the ground in the depth profile shown in Figure 3 reflect the lower temperature at depth, that functioned as a heat sink.

Figure 7 shows a strong inverse correlation, in the PG2 borehole, between the snow thickness and the soil surface energy exchange. The results show that once the snow height (m) reaches the maximum thickness, the permafrost becomes insulated from the atmospheric boundary layer during annual cycles.

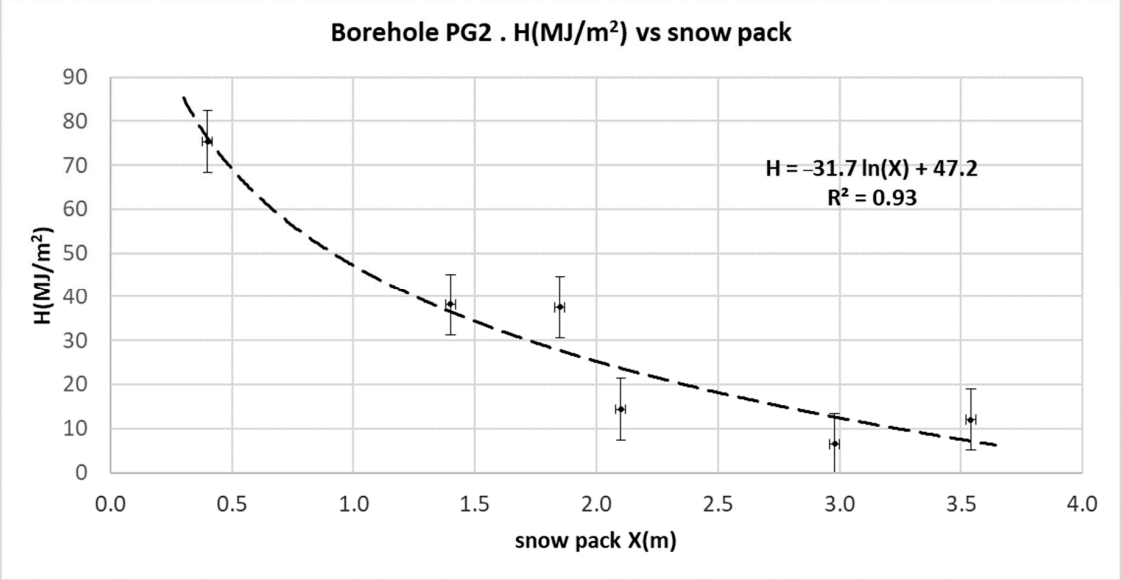

Figure 7. Correlation between the snow thickness and the soil surface energy exchange in PG2 and fit to a logarithmic function.

The behaviour of PG2 reflects a transition from a periglacial to a temperate glacial thermal regime, in which the active layer and freeze–thaw cycles typical of the periglacial domain completely disappeared [35]. The result was a ground thermal profile characterized by the reduction in the annual thermal amplitude at all depths, leading to a reduction in the total annual energy exchange (H), a decrease in the depth of the ZAA that approaches the interface ground-snow, and a complete disappearance of the active layer. Additionally, given the logarithmic fit between the dependence of the H versus the snow pack, which is presented in the Figure 7, the complete thermal isolation generated by the snow, H = 0 condition, correspond to a snow thickness of x~4.4 m.

Together with the known processes of glacial to periglacial transition associated with global warming, these observational data suggest that inverse processes (periglacial to glacial) may occur with increased snow accumulation over permafrost terrain. The typical permafrost thermal regime was here replaced to a subglacial thermal regime.

6. Conclusions

The analysis of the thermal regimes of two boreholes located about 300 m apart in the Reina Sofia Mount area from 2009 to 2015 in a period of increased snow has revealed remarkable differences between them. Both boreholes initially showed typical subaerial permafrost thermal regimes, with an active layer developing during the austral summer. Increased snow cover during the study period resulted in a thinning of the active layer at both sites. At PG2, located in a setting favourable for snow accumulation, the snowpack became over 3.5 m thick and permanent all year round. This resulted in the ground insulation from the atmosphere by the thick isothermal snowpack typical of the Maritime Antarctic. The presence of permafrost at depth acted as a heat sink, promoting surficial permafrost aggradation and the disappearance of the active layer. The analysis of the global energy exchange (H) in soil showed a high sensitivity to the buffering effect of the snowpack and that full insulation was reached once the snowpack surpassed ci. 4.4 m thick.

The short time-series from the Mount Reina Sofia boreholes reflects the thermal conditions of the quick transition from a subaerial to a subnival regime, which may be used as an analogue for transitions from a periglacial to a subglacial environment if longer periods of cooling in the paleoenvironmental record are to be considered.

Author Contributions: Data curation, M.R.; A.M. and J.J.J.; Investigation, M.R.; G.V.; M.A.d.P. and A.M.; Writing—original draft, M.R. and G.V.; Writing—review & editing, M.R., G.V. All authors have read and agreed to the published version of the manuscript.

Funding: This work has been supported by funds from the Ministry of Economy of the Government of Spain by the Polar Research Program (PERMAMODEL (POL2006-01918), PERMAPLANET (CTM2009-10165) and PERMASNOW (CTM2014-52021-R)) and PERMANTAR (PTDC/AAG-GLO/3908/2012) funded by PROPOLAR/FCT in Portugal. PG1 and PG2 boreholes have been jointly funded by the Gulbenkian Ambiente Program by mean of project PERMADRILL.

Acknowledgments: The authors thank the personnel of the Juan Carlos I Antarctic Station in Livingston Island for the support during field work.

Conflicts of Interest: The authors declare no conflict of interest.

Abbreviations and Units

ALT	Active Layer Thickness (m).
BAE JCI	Spanish Antarctic Station.
CALM	Circumpolar Active Layer Monitoring.
ERT	Electrical Resistivity Tomography.
GTN-P	Global Terrestrial Network for Permafrost.
IPY	International Polar Year.
MAAT	Mean Annual Air Temperature (°C).
PG1 and PG2	Permamodel-Gulbenkian boreholes 1 and 2.
TSP	Thermal State of Permafrost.
ZAA	Zero annual thermal amplitude (°C).
Symbols and units.	
x	spatial variable (m)
t	time variable (s)
α	thermal diffusivity (m^2/s)
H	Enthalpy (MJ/m^2)
k	thermal conductivity (W/m K)
T_M	annual maximum temperature distribution into the ground (°C)
T_m	annual minimum temperature distribution into the ground (°C)
X_{ALT}	ALT obtained from the Equation (3) (m)
X_{ZAA}	ZAA obtained from the Equation (5) (m)

References

1. Langer, M.; Wassermann, S.; Muster, S.; Piel, K.; Boike, J. Permafrost and surface energy balance of a polygonal tundra site in Northern Siberia. *Cryosphere Discuss* **2010**, *4*, 1391–1431. [CrossRef]
2. Zhang, T. Influence of the seasonal snow cover on the ground thermal regime: An overview. *Rev. Geophys.* **2005**, *43*, RG4002. [CrossRef]
3. Vieira, G.; Bockheim, J.; Guglielmin, M.; Balks, M.; Abramov, A.A.; Boelhouwers, J.; Cannone, N.; Ganzert, L.; Gilichinsky, D.A.; Goryachkin, S.; et al. Thermal state of permafrost and active-layer monitoring in the antarctic: Advances during the international polar year 2007–2009. *Permafr. Periglac. Process.* **2010**, *21*, 182–197. [CrossRef]
4. Biskaborn, B.K.; Smith, S.L.; Noetzli, J.; Matthes, H.; Vieira, G.; Streletskiy, D.A.; Schoeneich, P.; Romanovsky, V.E.; Lewkowicz, A.G.; Abramov, A.; et al. Permafrost is warming at a global scale. *Nat. Commun.* **2019**, *10*, 264. [CrossRef] [PubMed]
5. Bockheim, J.G. International Workshop on Antarctic Permafrost and Soils, November 14–18, 2004. In *Final Report Submitted to Office of Polar Programs, Antarctic Section, National Science Foundation, Project OPP-0425692*; University of Wisconsin: Madison, WI, USA, 2004.
6. Bockheim, J.; Vieira, G.; Ramos, M.; López-Martínez, J.; Serrano, E.; Guglielmin, M.; Wilhelm, K.; Nieuwendam, A. Climate warming and permafrost dynamics in the Antarctic Peninsula region. *Glob. Planet. Chang.* **2013**, *100*, 215–223. [CrossRef]

7. Staub, B.; Hasler, A.; Noetzli, J.; Delaloye, R. Gap-Filling Algorithm for Ground Surface Temperature Data Measured in Permafrost and Periglacial Environments Permafrost and Periglac. *Process* **2017**, *28*, 275–285. [CrossRef]
8. Ramos, M.; Vieira, G. Evaluation of the ground surface Enthalpy balance from bedrock temperatures (Livingston Island, Maritime Antarctic). *Cryosphere* **2009**, *3*, 133–145. [CrossRef]
9. Turner, J.; Barrand, N.E.; Bracegirdle, T.J.; Convey, P.; Hodgson, D.A.; Jarvis, M.; Jenkins, A.; Marshall, G.; Meredith, M.P.; Roscoe, H.; et al. Antarctic climate change and the environment: An update. *Polar Rec.* **2014**, *50*, 237–259. [CrossRef]
10. Turner, J.; Marshall, G.J.; Clem, K.; Colwell, S.; Phillips, T.; Lu, H. Antarctic Temperature Variability and Change from Station Data Article. *Int. J. Climatol.* **2019**. [CrossRef]
11. De Pablo, M.A.; Ramos, M.; Molina, A.; Vieira, G.; Hidalgo, M.A.; Prieto, M.; Jiménez, J.J.; Fernández, S.; Recondo, C.; Calleja, J.F.; et al. Frozen ground and snow cover monitoring in the South Shetland Islands, Antarctica: Instrumentation, effects on ground thermal behaviour and future research. *Cuad. Investig. Geográfica* **2016**, *42*, 475–495. [CrossRef]
12. Antarctic Climate Data READER Project. Available online: http://legacy.bas.ac.uk/met/READER (accessed on 1 December 2020).
13. de Pablo, M.A.; Ramos, M.; Molina, A. Snow cover evolution, on 2009–2014, at the Limnopolar Lake CALM-S site on Byers Peninsula, Livingston Island, Antarctica. *CATENA* **2017**, *149*, 538–547. [CrossRef]
14. Oliva, M.; Navarro, F.; Hrbáček, F.; Hernández, A.; Nývlt, D.; Pereira, P.; Ruiz-Fernández, J.; Trigo, R. Recent regional climate cooling on the Antarctic Peninsula and associated impacts on the cryosphere. *Sci. Total Environ.* **2017**, *580*, 210–223. [CrossRef] [PubMed]
15. Navarro, F.J.; Jonsell, U.Y.; Corcuera, M.I.; Martin-Espanol, A. Decelerated mass loss of Hurd and Johnsons Glaciers, Livingston Island, Antarctic Peninsula. *J. Glaciol.* **2013**, *59*, 115–128. [CrossRef]
16. Cook, A.J.; Vaughan, D.G.; Luckman, A.J.; Murray, T. A new Antarctic Peninsula glacier basin inventory and observed area changes since the 1940s. *Antarct. Sci.* **2014**, *26*, 614–624. [CrossRef]
17. Sancho, L.G.; Pintado, A.; Navarro, F.; Ramos, M.; De Pablo, M.A.; Blanquer, J.M.; Raggio, J.; Valladares, F.; Green, T.G.A. Recent Warming and Cooling in the Antarctic Peninsula Region has Rapid and Large Effects on Lichen Vegetation. *Sci. Rep.* **2017**, *7*. [CrossRef]
18. Ramos, M.; Vieira, G. Active layer and permafrost monitoring in Livingston Island, Antarctic. First results from 2000 to 2001. In Proceedings of the 8th International Conference on Permafrost, Zürich, Switzerland, 21–25 July 2003; pp. 929–933.
19. Hauck, C.; Vieira, G.; Gruber, S.; Blanco, J.; Ramos, M. Geophysical identification of permafrost in Livingston Island, maritime Antarctica. *J. Geophys. Res. Earth Surf.* **2007**, *112*, F02S19. [CrossRef]
20. Bañón, M.; Justel, A.; Velázquez, D.; Quesada, A. Regional weather survey on Byers Peninsula, Livingston Island, South Shetland Islands, Antarctica. *Antarct. Sci.* **2013**, *25*, 146–156. [CrossRef]
21. Bañon, M.; Vasallo, F. AEMET en la Antártida: Climatología y meteorología sinóptica en las estaciones meteorológicas españolas en la Antártida. *Agencia Estatal Meteorol.* **2015**. Available online: https://www.pinterest.co.uk/pin/390546598916668259/ (accessed on 5 December 2020).
22. Vieira, G.; López-Martínez, J.; Serrano, E.; Ramos, M.; Gruber, S.; Hauck, C.; Blanco, J.J. Geomorphological observations of permafrost and ground-ice degradation on Deception and Livingston Islands, Maritime Antarctica. In Proceedings of the 9th International Conference on Permafrost, Fairbanks, Alaska, 29 June–3 July 2008; pp. 1839–1844.
23. Molina, A.; de Pablo, M.A.; Ramos, M.; Vieira, G. Estudio del efecto de la cobertura nival sobre los periodos de congelación-descongelación en el entorno de la Base Antártica Española Juan Carlos, I. In *Criosferas, sueloscongelados y cambio climático. III Congreso Ibérico de la International Permafrost Association. Piornedo (Lugo, España)*; Departamento de Xeografía: Santiago de Compostela, Spain, 2011; pp. 87–92.
24. Ramos, M.; Hasler, A.; Vieira, G.; Hauck, C.; Gruber, S. Drilling and installation of boreholes for permafrost thermal monitoring on Livingston Island in the maritime Antarctic. *Permafr. Periglac. Process.* **2009**, *20*, 57–64. [CrossRef]
25. Correia, A.; Vieira, G.; Ramos, M. Thermal conductivity and thermal diffusivity of cores from a 26-meter-deep borehole drilled in Livingston Island, Maritime Antarctic. *Geomorphology* **2012**, *155–156*, 7–11. [CrossRef]

26. Romanovsky, V.E.; Drozdov, D.S.; Oberman, N.G.; Malkova, G.V.; Kholodov, A.L.; Marchenko, S.S.; Moskalenko, N.G.; Sergeev, D.O.; Ukraintseva, N.G.; Abramov, A.A.; et al. Thermal state of permafrost in Russia. *Permafrost Perigl. Process.* **2010**, *21*. [CrossRef]
27. Gubler, S.; Fiddes, J.; Keller, M.; Gruber, S. Scale-dependent measurement and analysis of ground surface temperature variability in alpine terrain. *Cryosphere* **2011**, *5*, 431–443. [CrossRef]
28. Lewkowicz, A.G. Evaluation of miniatures temperatures-loggers to monitor snow-pack evolution at mountain permafrost sites, northwestern Canada. *Permafr. Periglac. Process.* **2008**, *19*, 323–331. [CrossRef]
29. Danby, R.K.; Hik, D.S. Responses of white spruce (Picea glauca) to experimental warming at a subarctic alpine treeline. *Glob. Chang. Biol.* **2007**, *13*, 437–451. [CrossRef]
30. Osmanoglu, B.; Navarro Valero, F.J.; Hock, R.; Braun, M.; Corcuera Labrado, M.I. Surface velocity and mass balance of Livingston Island ice cap, Antarctica. *Cryosphere* **2014**, *8*, 1807–1823. [CrossRef]
31. Guglielmin, M.; Balks, M.R.; Adlam, L.S.; Baio, F. Permafrost thermal regime from two 30-m deep boreholes in southern victoria land. *Antarctica* **2011**, *22*, 129–139. [CrossRef]
32. Hrbáček, F.; Láska, K.; Engel, Z. Effect of Snow Cover on the Active-Layer Thermal Regime—A Case Study from James Ross Island. *Antarct. Penins.* **2016**, *27*, 307–315. [CrossRef]
33. Ramos, M.; de Pablo, M.A.; Vieira, G.; Molina, A.; Abramov, A.; Goyanes, G. Recent shallowing of the thaw depth at Crater Lake, Deception Island, Antarctica (2006–2014). *CATENA* **2017**, *149*, 519–528. [CrossRef]
34. Oliva, M.; Hrbacek, F.; Ruiz-Fernández, J.; de Pablo, M.A.; Vieira, G.; Ramos, M.; Antoniades, D. Active layer dynamics in three topographically distinct lake catchments in Byers Peninsula (Livingston Island, Antarctica). *CATENA* **2017**, *149*, 548–559. [CrossRef]
35. Ballantyne, C.K. Paraglacial geomorphology. *Quat. Sci. Rev.* **2002**, *21*, 1935–2017. [CrossRef]